

# Oceanography

THE OFFICIAL MAGAZINE OF THE OCEANOGRAPHY SOCIETY

## CITATION

Palevsky, H.I., and D.P. Nicholson. 2018. The North Atlantic biological pump: Insights from the Ocean Observatories Initiative Irminger Sea Array. *Oceanography* 31(1):42–49, <https://doi.org/10.5670/oceanog.2018.108>.

## DOI

<https://doi.org/10.5670/oceanog.2018.108>

## COPYRIGHT

This article has been published in *Oceanography*, Volume 31, Number 1, a quarterly journal of The Oceanography Society. Copyright 2018 by The Oceanography Society. All rights reserved.

## USAGE

Permission is granted to copy this article for use in teaching and research.

Republication, systematic reproduction, or collective redistribution of any portion of this article by photocopy machine, reposting, or other means is permitted only with the approval of The Oceanography Society. Send all correspondence to: [info@tos.org](mailto:info@tos.org) or The Oceanography Society, PO Box 1931, Rockville, MD 20849-1931, USA.

# The North Atlantic

## INSIGHTS FROM THE INITIATIVE IN

By Hilary LAPSLEY, **ABSTRACT**  
and David P. Nicholson



The biological pump plays a key role in the global carbon cycle by transporting photosynthetically fixed organic carbon into the deep ocean, where it can be sequestered from the atmosphere over annual or longer time scales if exported below the winter ventilation depth. In the subpolar North Atlantic, carbon sequestration via the biological pump is influenced by two competing forces: a spring diatom bloom that features large, fast-sinking biogenic particles, and deep winter mixing that requires particles to sink much further than in other ocean regions to escape winter ventilation. We synthesize biogeochemical sensor data from the first two years of operations at the Ocean Observatories Initiative Irminger SeaArray of moorings and gliders (September 2014–July 2016), providing the first simultaneous year-round observations of biological carbon cycling processes in both the surface ocean and the seasonal thermocline in this critical but previously undersampled region. These data show significant mixed layer net autotrophy during the spring bloom and significant respiration in the seasonal thermocline during the stratified season (~5.9 mol C mineralized between 200 m and 1,000 m). This respired carbon is subsequently ventilated during winter convective mixing (>1,000 m), a significant reduction in potential carbon sequestration. This highlights the importance of year-round observations to accurately constrain the biological pump in the subpolar North Atlantic, as well as other high-latitude regions that experience deep winter mixing.

Photo credit: Sheri White, © Woods Hole Oceanographic Institution

# INTRODUCTION

Current understanding suggests that it to the subtropical and tropical ocean (et al., 2012; Palevsky et al., 2016a). The anthropogenic carbon uptake to date has while high-latitude sites are sampled pre-rate of carbon sequestration below the been predominantly driven by the abi-dominantly during the spring and sumwinter ventilation depth depends not otic solubility pump as the surface ocean mer productive season. only on export from the euphotic zone

equilibrates with rising atmospheric CO<sub>2</sub>. Year-round sampling of the biological pump is especially critical in high-latitude regions because a large fraction of the carbon exported seasonally during the productive season but also during the subsequent winter. The depth of the thermocline and the depth of mixing are critical factors in determining the global rates of carbon transfer from the ocean.

global rate of carbon transfer from the surface to the deep ocean is about 100 Gt C yr<sup>-1</sup>.

face ocean to the interior via the biological pump, amounting to  $\sim$ 6–13 Pg C yr $^{-1}$

(Laws et al., 2011; Siegel et al., 2014), significantly exceed the current rate at which sinking particles consumed and superseded

The diagram illustrates the oxygen cycle in the ocean. A black line represents the oxygen minimum layer (OML) at approximately 1000 meters depth. A green dashed line shows the entrainment of oxygenated surface water into the OML. A green arrow indicates oxygen uptake by heterotrophic organisms, which is balanced by the entrainment of oxygenated water. The oxygen concentration is highest at the surface (~250 μM) and lowest at the OML (~100 μM).

estimated at  $2.6 \pm 0.5 \text{ Pg C}$  (Ye Quere et al., 2016), indicating that even a small reduction in the atmospheric concentration of CO<sub>2</sub> would result in a significant reduction in the atmospheric concentration of CO<sub>2</sub>.

perturbation to the biological pump could have a large influence on the global carbon cycle.

**FIGURE 1.** Schematic seasonal cycle of organic carbon export and winter ventilation in the North Atlantic (oxygen saturation and mixed layer depth based on World Ocean Atlas 2013 data for the GLO30\_0.25°\_Averge grid). Black dots on the thin lines indicate the locations of the

**the distribution of nutrients and oxygen in the ocean, with broad implications for the OOI Irmingen Sea Array site).** Phytoplankton growth in the spring and summer leads to export from the seasonally stratified mixed layer. This surface net autotrophy is evident in mixed layer oxygen supersaturation. However, much of the seasonally exported carbon is remineralized in the sea-

In order to effectively monitor and manage ocean ecosystems, it is essential to understand the complex interactions between the ocean and the atmosphere. The ocean's role in the global carbon cycle is particularly important, as it acts as a sink for atmospheric CO<sub>2</sub>. The ocean's ability to store CO<sub>2</sub> is influenced by factors such as temperature, salinity, and the presence of phytoplankton. The ocean's temperature and salinity are influenced by the atmosphere, and the atmosphere's temperature and salinity are influenced by the ocean. The ocean's phytoplankton populations are influenced by the availability of nutrients, which are often limited in the open ocean. The ocean's ecosystems are also influenced by human activities, such as fishing and shipping, which can have both positive and negative impacts on the environment.

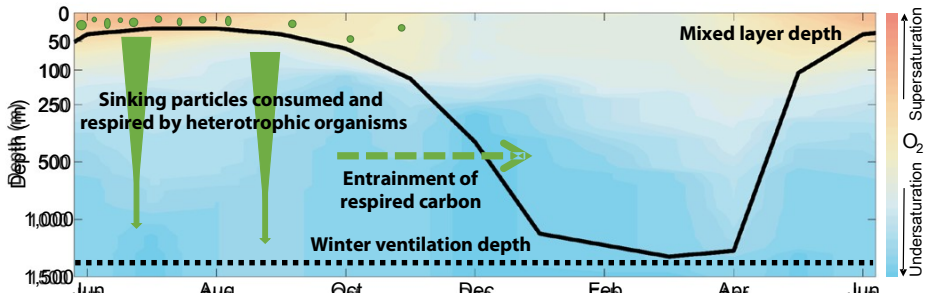


**FIGURE 1.** Schematic seasonal cycle of organic carbon export and winter ventilation in the North Atlantic (oxygen saturation and mixed layer depth based on World Ocean Atlas 2013 data for the OOI Irminger Sea Array site). Phytoplankton growth in the spring and summer leads to export from the seasonally stratified mixed layer. This surface net autotrophy is evident in mixed layer oxygen supersaturation. However, much of the seasonally exported carbon is remineralized in the seasonal thermocline and entrained back into the mixed layer during deep winter mixing. This ventilates the respiration carbon (and waters undersaturated with oxygen due to net respiration) back to the atmosphere. In order for carbon to be sequestered on annual or longer time scales, it must sink below the winter ventilation depth prior to remineralization.

In this paper, we focus on the Irminger et al., 2004; Khatiwala et al., 2009), mak-restratification (Dall'Olmo et al., 2016). Sea region of the subpolar North Atlanticing it a region of critical importance for However, this organic matter must pen- as a case study of the high-latitude biounderstanding the ocean's role in carbonetrate below the deepest winter mixing logical pump. The subpolar North cycling. Deepwater formation in the sub-depth in order not to be remineralized Atlantic is a strong carbon sink regiorpolar North Atlantic enhances the abilin the seasonal thermocline and venti- where the biological carbon pump's ity of the ocean to absorb carbon abiot- lated back to the atmosphere during the annual cycle features two pronounced ically via the solubility pump (Sabine subsequentwinter (Figure 1; Oschlies and competing processes: a spring dia to and Tanhua, 2010), and also increased Kahler, 2004; Körtzinger et al., 2008; bloom that produces large, fast sinking the sequestrationtime for biologically Quay et al., 2012). particles, and deep winter mixing that exported carbon that reaches below the The Irminger Sea, located between ventilates carbon remineralized in the winter ventilation depth (DeVries et al. Greenland and Iceland (Figure 2a), expe- seasonal thermocline back to the atm@2012). However, the amount of carboniences both the large spring bloom sphere (Figures 1 and )2a The Ocean sequesteredannually by the biological and deep winter mixing characteris- Observatories Initiative (OOI) Irminger pump and its role in driving ocean carbortic throughout the North Atlantic sub- Sea Array of moorings and gliders proptake in the subpolar North Atlantic is polar gyre. Strong wintertime atmo- vides a unique opportunity to study that well constrained (Sanders et al., 2014)pheric forcing over the Irminger Sea subpolar North Atlantic biological car- A dominant feature of the sub polarcools the surface ocean and drives bon pump throughout the year within the North Atlantic seasonal cycle is the large winter convective mixing to depths of context of an unprecedented density of atom-dominated spring phytoplank- up to 1,400 m, forming a water mass that biogeochemical, physical, and bio- opticabn bloom (Figure 2a; for a review of the extends throughout the mid-depth North sensors operating for multiple years abloom and its drivers, see Behrenfeld Atlantic (Pickart et al., 2003; de Jong high temporal resolution. We synthesize and Boss, 2014). Many prior stud- et al., 2012; de Jong and de Steur, 201 data from the OOI Irminger Sea Array's ies have documented high rates of de Jong et al., 2018, in this issue). There first two years of operation, illustratingmary production and organic carbon is significant interannual variability in the full annual cycle of biologically drivenexport from the surface ocean during the Irminger Sea convective mixing, with carbon cycling processes in both the sur-bloom (e.g., Buesseler et al., 1992; Quay the deepest mixing occurring during face ocean and the seasonal thermocline et al., 2012). Fast-sinking particles and years with the strongest surface cooling in this globally significant and previously aggregates can transfer this organic dassociated with the positive phase of the undersampled high-latitude region. bon to depth, with significant particle North Atlantic Oscillation; de Jong and

# THE SUBPOLAR NORTH ATLANTIC AND THE IRMINCH SEA

Anthropogenic carbon has accumulated in the North Atlantic at approximately three times the global average rate (Sabine et al., 2004). The latter can also be transferred from the surface mixed layer to the thermocline by episodic mixing followed by a delayed bloom and lower maximum concentrations in positive North Atlantic Oscillation years (Hanshaw et al., 2005).

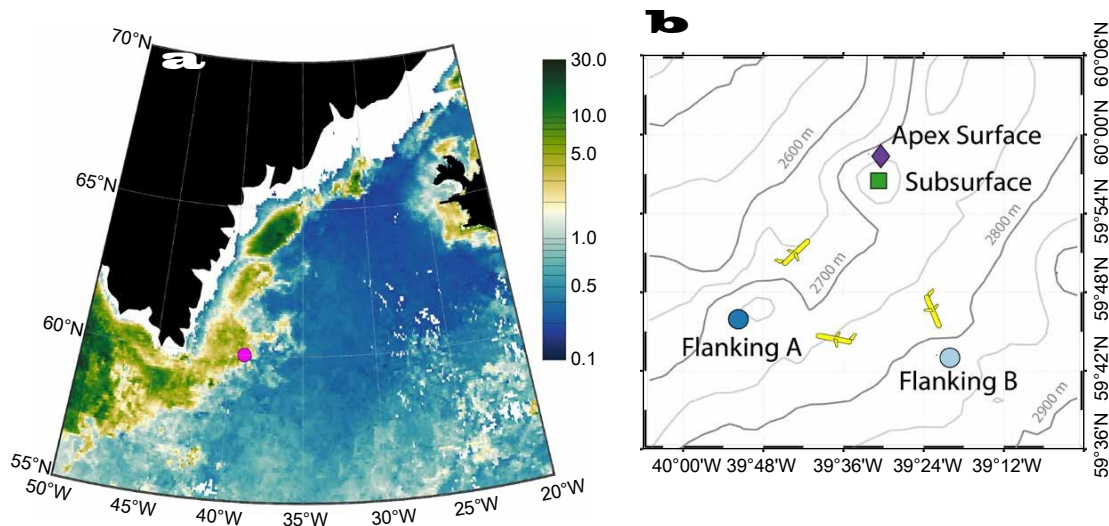


**FIGURE** (a) Sea surface chlorophyll a ( $\mu\text{g t}^{-1}$ ; 9 km MODIS Aqua) in the Irminger Sea from May 2015. The pink dot indicates the location of the OOI Irminger Sea Array. (b) Configuration of moorings and gliders at the OOI Irminger Sea Array, overlain on bathymetric contours.

that have stronger cooling and deeper optode model 4831 oxygen sensors are the gold standard for accurate dissolved mixing (Henson et al., 2006, 2009). This is located on all moorings and gliders oxygen measurements. This enables us to interannual variability in bloom dynamics within the OOI Array, and provide a con-to determine sensor-specific gain corrections and physical forcing likely also influence the amount of carbon seasonal surface and subsurface carbon cycling. We correct for in situ drift by assuming that oxygen exported from the surface ocean, remineralization rates in the seasonal thermocline, and the fraction of seasonally ventilated during winter on all moorings and gliders, and chlorophyll a concentrations determined from drift (Figure S2, Table S2).

not yet be disentangled, because long-surface mooring fluorometers (see online Supplementary Text for full details on all measurements are subject to greater uncertainty limited to physical properties and satellite data included in this analysis).

ocean color, without corresponding tracers of the biological pump. The picture of the Irminger Sea biological pump presented here, based on the first two years of data from the OOI Array, provides an initial snapshot of the system within the context of longer-term interannual variability, which this new time series enable us to resolve through continued collection of biogeochemical data over the coming years. Dissolved oxygen is a commonly used tracer of the biological pump because it records the balance between rates of oxygen production and respiration. In a net autotrophic system, production of organic carbon. Conversely, oxygen measurements will be

## DISSOLVED OXYGEN DATA FROM THE OOI ARRAY

Dissolved oxygen is a commonly used tracer of the biological pump because it records the balance between rates of oxygen production and respiration. In a net autotrophic system, production of organic carbon. Conversely, oxygen measurements will be

that is stoichiometrically related to net oxygen flux or net community production, which require highly accurate surface oxygen measurements (Emerson and Bushinsky, 2014). Further study with the coming years.

that is stoichiometrically related to net oxygen flux or net community production, which require highly accurate surface oxygen measurements (Emerson and Bushinsky, 2014). Further study with the coming years.

## OOI IRMINGER SEA ARRAY

The OOI Irminger Sea Array was first deployed in September 2014, beginning an ongoing time series of observations. The array is arranged in a triangular configuration (nominally 20 km a side), with an apex surface mooring co-located with a subsurface profiler mooring at the north point of the triangle and two flank moorings located at the southern cor-

ners (Figure 2b). Up to three open-ocean gliders continually transit around the array triangle, diving from the surface to 1,000 m. Annual summertime cruises recover all moorings and gliders from the previous year and deploy replacement, as well as conduct shipboard calibration casts for sensors on all moorings and gliders.

Here, we synthesize data collected over the first two years of OOI Irminger Sea Array deployment (September 2014–July 2016) to trace organic carbon production, remineralization, and ventilation. We focus in particular on dissolved oxygen, as stable response Aanderaa

Quantitative interpretation of dissolved oxygen sensor data requires that sensors be calibrated to account for two primary sources of error: (1) rapid drift of the Irminger Sea surface mixed layer oxygen data to depths of >1,000 m, as well as conduct shipboard calibration casts for sensors on all moorings and gliders.

Details of these corrections are provided in the Supplementary Text. We correct for pre-deployment drift using discrete samples for dissolved oxygen collected during the deployment. We focus in particular on dissolved oxygen, as stable response Aanderaa

face temperatures range from late winter minima of 3.5°–3.6°C to summer maximums of 9.5°C (Figure 3a). Previous analysis shows that the winter of 2014–2015 was characterized by exceptionally strong atmospheric forcing, as stable response Aanderaa board Winkler titrations, which remain associated with a high North Atlantic

## SEASONAL CYCLES IN THE SURFACE

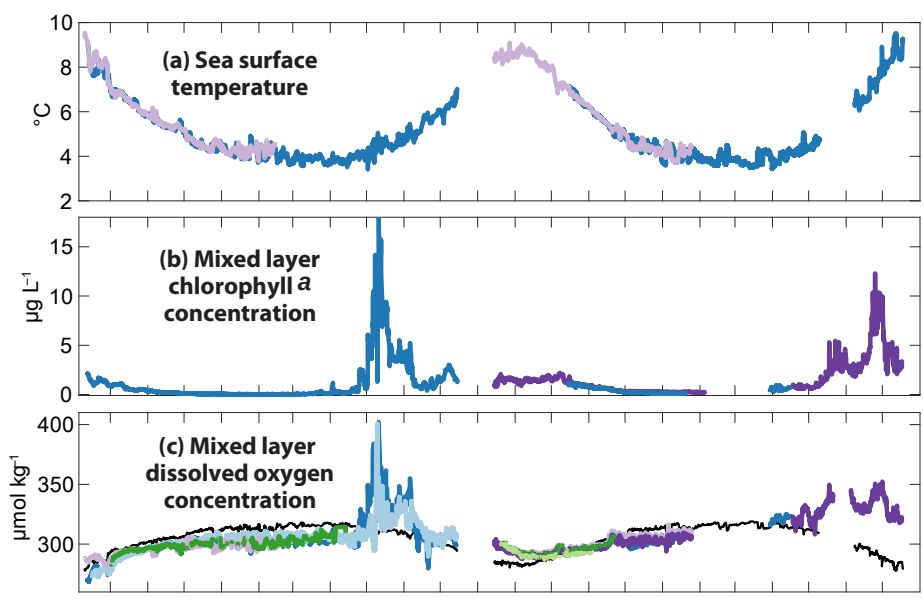
Seasonal cycles in physical, biological, and chemical properties (Figure 3). Sea surface temperatures range from late winter minima of 3.5°–3.6°C to summer maximums of 9.5°C (Figure 3a). Previous analysis shows that the winter of 2014–2015 was characterized by exceptionally strong atmospheric forcing, as stable response Aanderaa board Winkler titrations, which remain associated with a high North Atlantic

Oscillation index, which drove unusually strong surface cooling and deep wintén late April 2015, they remain super-saturated through early October. This, for similarly deep mixing in the winter of 2015/2016 (de Jong and de Steur, 2018, in this issue). The spring bloom is evident in elevated surface chlorophyll a concentrations from April to early June in both 2015 and 2016 (Figures 2a and 3b).

Observed mixed layer dissolved oxygen concentrations can be interpreted by comparison with oxygen concentrations expected if the surface ocean were in equilibrium with the atmosphere (equilibrium  $O_2$  in Figure 3c). Throughout the winter months, surface oxygen concentrations remain below saturation, indicating ventilation of oxygen-undersaturated deeper waters with a net increase in oxygen inventory places a respiration signature. Oxygen undersaturation persists until the beginning of the spring bloom, when surface oxygen rapidly increases in tandem with the increase in chlorophyll a. Once oxygen

reaches supersaturation of 1.4; Laws, 1991). Previous estimates of subpolar North Atlantic spring bloom are of comparable magnitude (Quay et al., 2012, and references therein), suggesting that the total NCP during the bloom is likely considerably greater than our lower bound estimate.

## SEASONAL CYCLES IN THE THERMOCLINE AND WINTER VENTILATION



- Equilibrium  $O_2$
- Flanking Mooring A
- Flanking Mooring B
- Apex Mooring (~12 m)
- Apex Mooring (~1 m)
- Glider 002
- Glider 003

**FIGURE 3.** Surface mixed layer (a) sea surface temperature, (b) chlorophyll a concentration, and (c) dissolved oxygen from the OOI Irminger Sea Array over the first two years of deployment. Data are compiled from multiple array assets (see Figure 2b) to provide nearly continuous data. The oxygen concentration expected if the mixed layer were in equilibrium with the atmosphere, calculated from sea surface temperature and salinity following the equation of Garcia and Gordon (1992), is provided in (c) for comparison with observed concentrations.

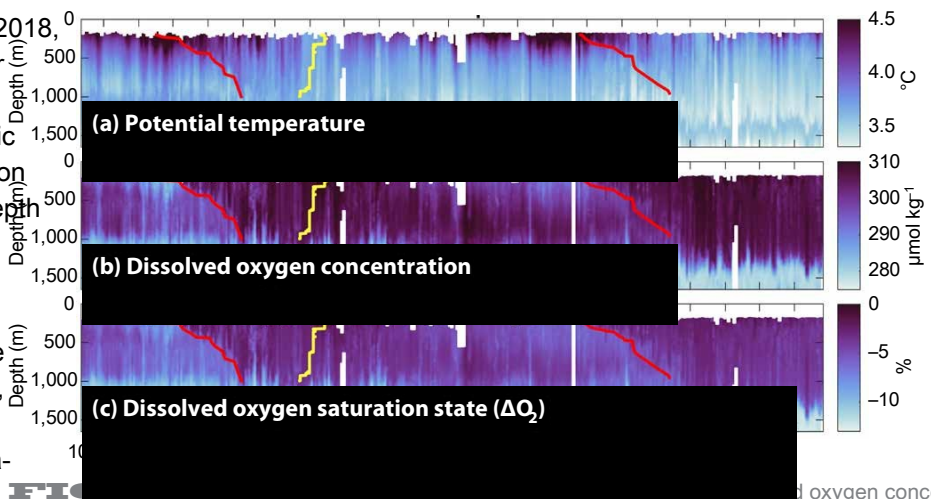
Observations below the mixed layer allow us to see the seasonal evolution of respiration and ventilation within the seasonal thermocline. Profiler mooring temperature data (Figure 4a) were compared to a maximum value of  $402 \mu\text{mol kg}^{-1}$  on May 11 reflects an increase in the mixed layer oxygen inventory of  $\sim 3.0 \text{ mol m}^{-2}$  with sea surface temperature (Figure 3a) integrated through the  $\sim 30 \text{ m}$  mixed layer to determine the base of the mixed layer at the time of the oxygen maximum. This  $\Delta 0.2^\circ\text{C}$  from the sea surface temperature; de Boyer Montégut et al., 2004). lower bound (neglecting oxygen flux to) during the stratified spring and summer season, the profiler mooring's surface measurements are well below the mixed layer (i.e., the uppermost temperature measurements from the profiler mooring are more than  $0.2^\circ\text{C}$  cooler than the sea surface). As the mixed layer deepens in fall and winter, the surface mixed layer penetrates into the seasonal thermocline and ventilates waters that were isolated from contact with the atmosphere during the stratified season. In both 2014 and 2015, mixed layers first reached to 200 m depth in mid-November, with ventilation extending deeper into the water column and progressively eroding seasonal stratification through the winter (red lines in Figure 4).

The dates of initial winter ventilation (the time that the mixed layer first penetrates to a given depth within the thermocline) correspond with a rapid increase in dissolved oxygen concentration at depth as the oxygen-undersaturated thermocline waters are exposed to the atmosphere (Figure 4b,c). Once ventilation has penetrated to a given depth, oxygen concentrations at that depth continue to increase throughout the period of winter convection until stratification is reestablished in spring (Figure 5). Because the

depth of active mixing often decreases in then ventilated back to the atmosphere (Palevsky et al., 2016a), consistent with the spring prior to stratification of the mixed during winter. Integrated through the Irminger Sea's stronger spring bloom and layer defined based on physical properties, the 200–1,000 m layer within the seasonal deeper winter mixing that enhances the ties, the date of re-stratification in spring thermocline, ~5.9 mol C m<sup>-2</sup> was remineralized (8.3 mol Q m<sup>-2</sup> consumed by the yellow lines in Figure 4). The importance of thermocline remineralization and winter ventilation.

Respiration in the seasonal thermo-in 2015/2016. This magnitude of winter pump can be thought of as a “tug of cline is evident in the oxygen decrease ventilation is greater than that previously war” between downward flux of organic over the stratified season (Figure 5). These observed in other deep mixing regions scatter from the surface during the strat-layers are isolated from contact with the (2.6 mol C m<sup>-2</sup> in the eastern North ified productive season and upward flux atmosphere, and the seasonal-scale influAtlantic and 3.6 mol C m<sup>-2</sup> in the west- of remineralized organic matter during ence of advection is low because the proern North Pacific; Körtzinger et al., 2008; wintertime ventilation. Both of these filer mooring is located near the cen- ter of the gyre where the mean currents

Consistent with previous oxygen-based estimates of subsurface respiration (Martz et al., 2008; Hennon et al., 2016) and with canonical expectations for attenuation of organic matter flux with depth (J.M. Martin et al., 1987), total seasonal respiration is greatest near the top of the thermocline and decreases with depth (Figure 6). The duration of the stratified season over which this respiration occurs increases with depth, as re-stratification begins earlier and winter ventilation begins later deeper in the water column (stratification duration ranges from  $194 \pm 1$  days at depths from 200–300 m to  $280 \pm 3$  days at depths from 750–1,000 m; Figures 4 and 5). The total respiration within each depth interval is stoichiometrically related to an increase in dissolved inorganic carbon due to organic matter remineralization over the course of the stratified season, which is



solved oxygen saturation state (Equation 1):

$$(\Delta O_2 = \left( \frac{O_2, \text{observed}}{O_2, \text{equilibrium}} - 1 \right) * 100)$$

from the profiler mooring. Red lines indicate the beginning of winter ventilation in each year (determined as the time that the mixed layer first penetrates to a given depth), and yellow lines indicate the end of winter ventilation in 2015 (determined as the date of the late winter-early spring oxygen maximum at each depth; see Figure 5).

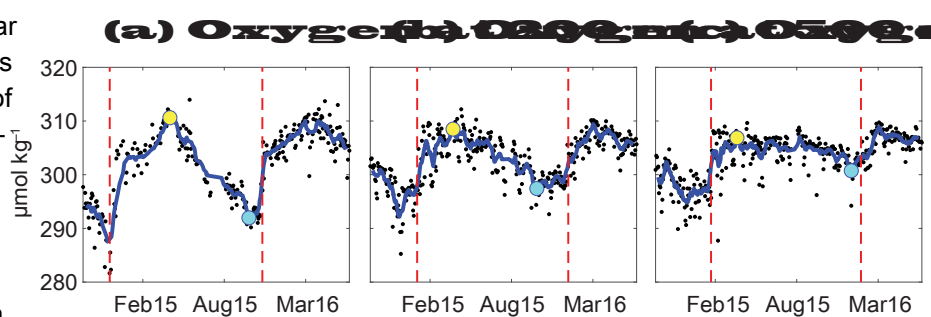


**FIGURE 5.** Examples of dissolved oxygen time series at (a) 200 m, (b) 500 m, and (c) 800 m from the profiler mooring over the first two years' deployment of the OOI Irminger Sea Array. Blue lines show the smoothed time series, determined as a 10-point filtered mean of all dissolved oxygen values gridded to each depth (black points). Red dashed lines indicate the date of initial winter ventilation in each year, determined as the time that the mixed layer first penetrates to the given depth. The end of winter ventilation (cyan dots) in spring 2015 is determined as the maximum dissolved oxygen concentration. The oxygen decrease from the end of winter ventilation (yellow dots) to the minimum oxygen concentration at the end of the stratified season (cyan dots) shows respiration of inorganic carbon within the seasonal thermocline.

# CONCLUSIONS

the mixed layer during winter ventilation Carbon sequestration via the biological

-in 2015/2016. This magnitude of winter pump can be thought of as a “tug of ventilation is greater than that previously war” between downward flux of organic observed in other deep mixing regions matter from the surface during the strat- (2.6 mol C m<sup>-2</sup> in the eastern North Atlantic and 3.6 mol C m<sup>-2</sup> in the west- ified productive season and upward flux of remineralized organic matter during northern North Pacific; Körtzinger et al., 2008; wintertime ventilation. Both of these

## Total stratified season respiration

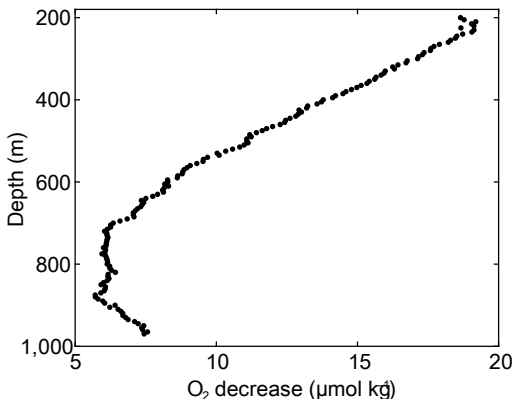


**FIGURE 6.** Total respiratory oxygen decrease in the seasonal thermocline (200–1,000 m depth) over the 2015 stratified season, calculated as the oxygen decrease from the end of winter ventilation in spring 2015 to the oxygen minimum at the end of the stratified season (from the yellow to the cyan dots in Figure 5). Thermocline respiration integrated through this full layer is 8.3 mol O<sub>2</sub> m<sup>-2</sup>, representing 5.9 mol C m<sup>-2</sup> ventilated back to the atmosphere the subsequent winter (O<sub>2</sub>:C ratio of 1.4; Laws, 1991).

cycling throughout the full annual cycle in the previously undersampled high-latitude ocean.

## SUPPLEMENTARY

Supplementary Text, Figures S1 and S2, and Tables S1 and S2, include details on all data used in this analysis and are available online at <https://doi.org/10.5670/oceanog.2018.108>.

## REFERENCES

Antia, N., R. Peinert, D. Hebbeln, U. Bathmann, U. Fehner, and B. Zeitzschel. 2001. Basin-wide particulate carbon flux in the Atlantic Ocean: Regional export patterns and potential for atmospheric CO<sub>2</sub> sequestration. *Global Biogeochemical Cycles* 15(4):845–862, <https://doi.org/10.1029/2000gb001376>.

Behrenfeld, M.J., and E.S. Boss. 2014. Resurrecting the ecological underpinnings of ocean plankton blooms. *Annual Review of Marine Science* 6(1):167–194, <https://doi.org/10.1146/annurev-marine-052913-021325>.

Bittig, H.C., and A. Körtzinger. 2015. Tackling oxygen optode drift: Near-surface and in-air oxygen optode measurements on a float provide an accurate in situ reference. *Journal of Atmospheric and Oceanic Technology* 32(8):1,536–1,543, <https://doi.org/10.1175/JTECH-D-14-00162.1>.

Bittig, H.C., and A. Körtzinger. 2017. Technical note: Update on response times, in-air measurements, and in situ drift for oxygen optodes on profiling platforms. *Ocean Science* 13(1):1–11, <https://doi.org/10.5194/os-13-1-2017>.

Briggs, N., M.J. Perry, I. Cetinić, C. Lee, E. D'Asaro, A.M. Gray, and E. Rehm. 2011. High-resolution observations of aggregate flux during a sub-polar North Atlantic spring bloom. *Deep Sea Research Part I* 58(10):1,031–1,039, <https://doi.org/10.1016/j.dsr.2011.07.007>.

Buesseler, K.O., P. Michael, H.D. Livingston, and K. Cochran. 1992. Carbon and nitrogen export during the JGOFS North Atlantic Bloom Experiment estimated from <sup>234</sup>Th-<sup>238</sup>U disequilibria. *Deep Sea Research* 39(7–8):1,115–1,137, [https://doi.org/10.1016/0198-0149\(92\)90060-7](https://doi.org/10.1016/0198-0149(92)90060-7).

Bushinsky, S.M., S.R. Emerson, S.C. Riser, and D.D. Swift. 2016. Accurate oxygen measurements on modified Argo floats using in situ air calibrations. *Limnology and Oceanography: Methods* 14:491–505, <https://doi.org/10.1002/lom3.10107>.

Claire, M.J., M.W. Lomas, and F. Muller-Karger. 2013. Sea change: Charting the course for biogeochemical ocean time-series research in a new millennium. *Deep Sea Research Part II* 93:2–15, <https://doi.org/10.1016/j.dsr2.2013.01.035>.

Ciais, P., C. Sabine, G. Bala, L. Bopp, V. Brovkin, J. Canadell, A. Chhabra, R. DeFries, J. Galloway, M. Heimann, and others. 2013. Carbon and other biogeochemical cycles. Pp. 465–570. In *Climate Change 2013 - The Physical Science Basis. Contribution of Working Group I to the Fifth Assessment Report of the Intergovernmental Panel on Climate Change*. T.F. Stocker, D. Qin, G.-K. Plattner, M. Tignor, S.K. Allen, J. Boschung, A. Nauels, Y. Xia, and V. Bex, eds, Cambridge University Press, Cambridge, United Kingdom and New York, NY, USA, <https://doi.org/10.1017/CBO9781107415324.015>.

D'Asaro, E.A., and C. McNeil. 2013. Calibration and stability of oxygen sensors on autonomous floats. *Journal of Atmospheric and Oceanic Technology* 30:1,896–1,906, <https://doi.org/10.1175/JTECH-D-12-00222.1>.

Dall'Olmo, G., J. Dingle, L. Polimene, R.J.W. Brewin, and H. Claustre. 2016. Substantial energy input to the mesopelagic ecosystem from the seasonal mixed-layer pump. *Nature Geoscience* 9:820–823, <https://doi.org/10.1038/ngeo2818>.

players “tug” especially hard in the subpolar North Atlantic (Figure 1). Data from the first two years of the new OOI Irminger Sea Array provide the first simultaneous observations of the seasonal progression of the biological pump in both the surface mixed layer and the seasonal thermocline in the subpolar North Atlantic Ocean. The spring bloom from the Irminger Sea and other OOI during April–May each year was associated with a dramatic increase in mixed layer dissolved oxygen, reflecting significant net autotrophic production during profiles (Nicholson and Feen, 2017), and this period (Figures 2 and 3). Below the mixed layer, oxygen decline over the 2015 stratified season indicated high remineralization rates within the seasonal thermocline totaling ~5.9 mol C m<sup>-2</sup> between 200 m and 1,000 m—greater than the total annual export from the surface in most parts of the ocean (Figures 5 and 6; Emerson, 2014). Deep winter convection (de Steur, 2016), future observations of convection extending below 1,000 m will play an important role in contextualizing this respiration signature from the seasonal thermocline, maintaining surface biological pump presented here. Face dissolved oxygen concentrations Ongoing time-series observations at the below saturation throughout the winter OOI Array, ideally with improved calibration of biogeochemical sensors, will act to return mixed layer oxygen to aenable future analysis of interannual variability in the timing and magnitude

These results highlight the importance of accounting for remineralization within the seasonal thermocline and ventilation of respiration carbon back to the atmosphere-winter ventilation. Biogeochemical sensors during winter mixing in order to accurately determine the influence of the biological pump on carbon sequestration items (e.g., Biogeochemical Argo floats) particularly in deep convection regions (Johnson and Claustre, 2016) provide such as the Irminger Sea. However, a powerful tool for investigating carbon

de Boyer Montégut, C., G. Madec, A.S. Fischer, A. Lazar, and D. Iudicone. 2004. Mixed layer depth over the global ocean: An examination of profile data and a profile-based climatology. *Journal of Geophysical Research* 109, C12003, <https://doi.org/10.1029/2004JC002378>.

de Jong, M.F., and L. de Steur. 2016. Strong winter cooling over the Irminger Sea in winter 2014–2015, exceptional deep convection, and the emergence of anomalously low SST. *Geophysical Research Letters* 43(13):7,106–7,113, <https://doi.org/10.1002/2016GL069596>.

de Jong, M.F., M. Oltmanns, J. Karstensen, and L. de Steur. 2018. Deep convection in the Irminger Sea observed with a dense mooring array. *Oceanography* 31(1):50–59, <https://doi.org/10.5670/oceanog.2018.109>.

de Jong, M.F., H.M. Van Aken, K. Våge, and R.S. Pickart. 2012. Convective mixing in the central Irminger Sea: 2002–2010. *Deep Sea Research Part I* 63:36–51, <https://doi.org/10.1016/j.dsr.2012.01.003>.

DeVries, T., F. Primeau, and C. Deutsch. 2012. The sequestration efficiency of the biological pump. *Geophysical Research Letters* 39, L13601, <https://doi.org/10.1029/2012GL051963>.

Emerson, S. 2014. Annual net community production and the biological carbon flux in the ocean. *Global Biogeochemical Cycles* 28:14–28, <https://doi.org/10.1002/2013GB004680>.

Emerson, S., and S. Bushinsky. 2014. Oxygen concentrations and biological fluxes in the open ocean. *Oceanography* 27(1):168–171, <https://doi.org/10.5670/oceanog.2014.20>.

Field, C.B., M.J. Behrenfeld, J.T. Randerson, and P. Falkowski. 1998. Primary production of the biosphere: Integrating terrestrial and oceanic components. *Science* 281(5374):237–240, <https://doi.org/10.1126/science.281.5374.237>.

Garcia, H.E., and L.I. Gordon. 1992. Oxygen solubility in seawater: Better fitting solubility equations. *Limnology and Oceanography* 37(6):1,307–1,312, <https://doi.org/10.4319/lo.1992.37.6.1307>.

Hennon, T.D., S.C. Riser, and S. Mecking. 2016. Profiling float-based observations of net respiration beneath the mixed layer. *Global Biogeochemical Cycles* 30:920–932, <https://doi.org/10.1002/2016GB005380>.

Henson, S.A., C. Beaufieu, and R. Lampitt. 2016. Observing climate change trends in ocean biogeochemistry: When and where. *Global Change Biology* 22:1,1561–1,1571, <https://doi.org/10.1111/gcb.13152>.

Henson, S.A., J.P. Dunne, and J.L. Sarmiento. 2009. Decadal variability in North Atlantic phytoplankton blooms. *Journal of Geophysical Research* 114(4):1–11, <https://doi.org/10.1029/2008JC005139>.

Henson, S.A., I. Robinson, J.T. Allen, and J.J. Waniek. 2006. Effect of meteorological conditions on interannual variability in timing and magnitude of the spring bloom in the Irminger Basin, North Atlantic. *Deep Sea Research Part I* 53:1,601–1,615, <https://doi.org/10.1016/j.dsr.2006.07.009>.

Johnson, K.S., and H. Claustre. 2016. Bringing Biogeochemistry into the Argo Age. *Eos* 97, <https://doi.org/10.1029/2016EO062427>.

Johnson, K.S., J.N. Plant, S.C. Riser, and D. Gilbert. 2015. Air oxygen calibration of oxygen optodes on a profiling float array. *Journal of Atmospheric and Oceanic Technology* 32(11):2,160–2,172, <https://doi.org/10.1175/JTECH-D-15-0101.1>.

Khatiwala, S., F. Primeau, and T. Hall. 2009. Reconstruction of the history of anthropogenic CO<sub>2</sub> concentrations in the ocean. *Nature* 462(7271):346–349, <https://doi.org/10.1038/nature08526>.

Körtzinger, A., U. Send, R.S. Lampitt, S. Hartman, D.W.R. Wallace, J. Karstensen, M.G. Villagarcia, O. Llinás, and M.D. DeGrandpre. 2008. The seasonal pCO<sub>2</sub> cycle at 49°N/16.5°W in the north-eastern Atlantic Ocean and what it tells us about biological productivity. *Journal of Geophysical Research* 113, C04020, <https://doi.org/10.1029/2007JC004347>.

Laws, E.A. 1991. Photosynthetic quotients, new production and net community production in the open ocean. *Deep Sea Research* 38(1):143–167, [https://doi.org/10.1016/0198-0149\(91\)90059-O](https://doi.org/10.1016/0198-0149(91)90059-O).

Laws, E.A., E. D'Sa, and P. Naik. 2011. Simple equations to estimate ratios of new or export production to total production from satellite-derived estimates of sea surface temperature and primary production. *Limnology and Oceanography: Methods* 9:593–601, <https://doi.org/10.4319/lom.2011.9.593>.

Le Quéré, C., R.M. Andrew, J.G. Canadell, S. Sitch, J.I. Korsbakken, G.P. Peters, A.C. Manning, T.A. Boden, P.P. Tans, R.A. Houghton, and others. 2016. Global carbon budget 2016. *Earth System Science Data* 8:605–649, <https://doi.org/10.5194/essd-8-605-2016>.

Martin, J.M., G.A. Knauer, D.M. Karl, and W.W. Broenkow. 1987. VERTEX: Carbon cycling in the Northeast Pacific. *Deep Sea Research* 34(2):267–285, [https://doi.org/10.1016/0198-0149\(87\)90086-0](https://doi.org/10.1016/0198-0149(87)90086-0).

Martin, P., R.S. Lampitt, M.J. Perry, R. Sanders, C. Lee, and E. D'Asaro. 2011. Export and mesopelagic particle flux during a North Atlantic spring diatom bloom. *Deep Sea Research Part I* 58:338–349, <https://doi.org/10.1016/j.dsr.2011.01.006>.

Martz, T.R., K.S. Johnson, and S.C. Riser. 2008. Ocean metabolism observed with oxygen sensors on profiling floats in the South Pacific. *Limnology and Oceanography* 53(5, part 2):2,094–2,111, [https://doi.org/10.4319/lo.2008.53.5\\_part\\_2.2094](https://doi.org/10.4319/lo.2008.53.5_part_2.2094).

Nicholson, D.P., and M.L. Feen. 2017. Air calibration of an oxygen optode on an underwater glider. *Limnology and Oceanography: Methods* 15:495–502, <https://doi.org/10.1002/lim3.10177>.

Oschlies, A., and P. Kahler. 2004. Biotic contribution to air-sea fluxes of CO<sub>2</sub> and O<sub>2</sub> and its relation to new production, export production, and net community production. *Global Biogeochemical Cycles* 18, GB1015, <https://doi.org/10.1029/2003GB002094>.

Palevsky, H.I., P.D. Quay, D.E. Lockwood, and D.P. Nicholson. 2016a. The annual cycle of gross primary production, net community production, and export efficiency across the North Pacific Ocean. *Global Biogeochemical Cycles* 30:361–380, <https://doi.org/10.1002/2015GB005318>.

Palevsky, H.I., P.D. Quay, and D.P. Nicholson. 2016b. Discrepant estimates of primary and export production from satellite algorithms, a biogeochemical model and geochemical tracer measurements in the North Pacific Ocean. *Geophysical Research Letters* 43:8,645–8,653, <https://doi.org/10.1002/2016GL070226>.

Pickart, R.S., M.A. Spall, M.H. Rønberg, G.W.K. Moore, and R.F. Milliff. 2003. Deep convection in the Irminger Sea forced by the Greenland tip jet. *Nature* 424(6945):152–156, <https://doi.org/10.1038/nature01729>.

Quay, P., J. Stutsman, and T. Steinhoff. 2012. Primary production and carbon export rates across the subpolar N. Atlantic Ocean basin based on triple oxygen isotope and dissolved O<sub>2</sub> and Ar gas measurements. *Global Biogeochemical Cycles* 26, GB2003, <https://doi.org/10.1029/2010GB004003>.

Sabine, C.L., R.A. Feely, N. Gruber, R.M. Key, K. Lee, J.L. Bullister, R. Wanninkhof, C. Wong, D.W.R. Wallace, B. Tilbrook, and others. 2004. The oceanic sink for anthropogenic CO<sub>2</sub>. *Science* 305:367–371, <https://doi.org/10.1126/science.1097403>.

Sabine, C.L., and T. Tanhua. 2010. Estimation of anthropogenic CO<sub>2</sub> inventories in the ocean. *Annual Review of Marine Science* 2:175–198, <https://doi.org/10.1146/annurev-marine-120308-080947>.

Sanders, R., S.A. Henson, M. Koski, C.L. De La Rocha, S.C. Painter, A.J. Poulton, J. Riley, B. Salihoglu, A. Visser, A. Yool, and others. 2014. The biological carbon pump in the North Atlantic. *Progress in Oceanography* 129:200–218, <https://doi.org/10.1016/j.pocean.2014.05.005>.

Sarmiento, J.L., and N. Gruber. 2006. *Ocean Biogeochemical Dynamics*. Princeton University Press, Princeton, NJ, 526 pp.

Siegel, D.A., K.O. Buesseler, S.C. Doney, S.F. Sallie, M.J. Behrenfeld, and P.W. Boyd. 2014. Global assessment of ocean carbon export by combining satellite observations and food-web models. *Global Biogeochemical Cycles* 28:181–196, <https://doi.org/10.1002/2013GB004743>.

Stukel, M.R., M. Kahru, C.R. Benitez-Nelson, M. Decima, R. Goericke, M.R. Landry, and M.D. Ohman. 2015. Using Lagrangian-based process studies to test satellite algorithms of vertical carbon flux in the eastern North Pacific Ocean. *Journal of Geophysical Research* 120:7,208–7,222, <https://doi.org/10.1002/2015JC011264>.

Takeshita, Y., T.R. Martz, K.S. Johnson, J.N. Plant, D. Gilbert, S.C. Riser, C. Neill, and B. Tilbrook. 2013. A climatology-based quality control procedure for profiling float oxygen data. *Journal of Geophysical Research* 118:5,640–5,650, <https://doi.org/10.1029/jgrc.20399>.

Volk, T., and M.I. Hoffert. 1985. Ocean carbon pumps: Analysis of relative strengths and efficiencies in ocean-driven atmospheric CO<sub>2</sub> changes. Pp. 99–110 in *The Carbon Cycle and Atmospheric CO<sub>2</sub> Natural Variations Archean to Present*. E.T. Sundquist and W.S. Broecker, eds, Geophysical Monograph Series, vol. 32, American Geophysical Union, Washington, DC.

## ACKNOWLEDGMENT

We are grateful to the many people involved in the planning, deployment, operation, and data management of the Ocean Observatories Initiative, and to the National Science Foundation for OOI funding. We thank Robert Weller, Paul Quay, Robert Vaillancourt, and an anonymous reviewer for constructive feedback that improved the manuscript. Hilary Palevsky acknowledges support from the Postdoctoral Scholar Program at the Woods Hole Oceanographic Institution, with funding provided by the Weston Howland Jr. Postdoctoral Scholarship.

## AUTHORS

**Hilary I. Palevsky** (hpalevsky@whoi.edu) Postdoctoral Scholar and **David P. Nicholson** Associate Scientist, both in the Department of Marine Chemistry and Geochemistry, Woods Hole Oceanographic Institution, Woods Hole, MA, USA.

## ARTICLE CITATION

Palevsky, H.I., and D.P. Nicholson. 2018. The North Atlantic biological pump: Insights from the Ocean Observatories Initiative Irminger Sea Array. *Oceanography* 31(1):42–49, <https://doi.org/10.5670/oceanog.2018.108>.